Trajectory Tracking of Rotating Shaft with Active Magnetic Bearings under Different Reference Signals

Xudong Guan, Jin Zhou, Haitong Wu, and Yue Zhang

College of Mechanical and Electrical Engineering
Nanjing University of Aeronautics and Astronautics, Nanjing 210016, China
guanxd@nuaa.edu.cn, zhj@nuaa.edu.cn, wu_haitong@163.com, haianzy95@126.com

Abstract **–** Using magnetic levitation technology to implement a reference signal can avoid fluid mechanical surge and better control the movement of motorized spindle-mounted cutting tools. Magnetic levitation has the advantages of no friction, no mechanical wear, and high efficiency. In this paper, the performance of axial trajectory tracking control of active magnetic bearings with a classical proportional-integral-derivative (PID) controller is studied. First, the principles of trajectory tracking with an active magnetic bearing system are expounded, and the mechatronics models of such a system are established. Then, a PID controller is designed and trajectory tracking performance using different reference signals is verified by simulation and experiment. The results show that PID-based control of magnetic bearings can meet the requirements of tracking position control. In the experiments, the tracking errors were all within 18 μm in the rotating state.

Index Terms **–** Active magnetic bearings, machining movement, mechatronics modeling, reference signal, trajectory tracking.

I. INTRODUCTION

Magnetic levitation technology has been widely used in rotating machinery for its advantages of having no mechanical contact or wear, zero friction, long service life, no lubrication, high efficiency, and low noise [1]. In recent years, it has been applied to active magnetic bearings (AMBs) and maglev trains. It is also gradually being applied in trajectory tracking control, such as fluid mechanical surge suppression and the tracking of motorized spindle machining tools.

Tooltip tracking refers to the use of a reference signal as a guide for the machining of parts with complex geometries. In previous work, tooltip tracking has been implemented with ball screw mechanisms [2, 3] and actuators [4, 5]. In the present study [6], a synchronous tool tracking method for an AMB rigid rotor with invariant control is proposed. Wang [7] put forward a principle for machining noncircular piston pin-holes by controlling the trajectory of the spindle's axis to achieve high-frequency and radial micromotions. Smirnov [8] adopted tool tracking in AMB spindle and adjusted magnetic bearings through a PID control strategy, which enables the tool to reach a set position. Classical PID control methods are very practical due to their clear physical concepts and intuitive design processes. However, they require a high level of knowledge and insights in the fields of system dynamics and classical control [9]. Sanadgol [10] and Yoon [11] achieved surge control in a magnetic suspension centrifugal compressor by using the H_∞ robust control method, which mainly depends on the adjustment of the rotor's axial position; that is, axial trajectory tracking control of the rotor. Minihan [12] investigated the variation in electromagnetic forces at different levitation positions for large displacement tracking control of magnetic bearings and designed three kinds of nonlinear controllers to achieve position tracking control. Pesch [13] and others studied the rotor position tracking performance of radial magnetic bearings based on μ-synthesis. Reference [14] proposed an adaptive tracking method that ensures stable operation throughout the rotational speed range. Grochmal [15] introduced a nonlinear reduced-order disturbance observer and applied it to flatness-based tracking control. In reference [16], an adaptive control algorithm was applied to the suspension system of a single-degree-of-freedom magnetic bearing system. It proved valuable in the design and implementation of a precise positioning platform based on this magnetic bearing system. In summary, many scholars have studied the trajectory tracking control of AMBs, but few have studied tracking performance under different reference signals, which is also very important. Therefore, it is necessary to track the trajectory of AMBs under different reference signals. Furthermore, it is particularly important to ensure that a bearing rotor has good positional tracking performance under different reference signals in the process of axial position tracking control. In this process, the magnetic thrust bearings need to drive a rotor and change its axial position to meet the needs of different reference signals (part contours).7

Based on the above research, in this paper, a PID

Submitted On: November 28, 2018
Accepted On: April 6, 2019

controller is applied to a magnetic thrust bearing to study the positional tracking of AMBs. The main contribution of this paper is to study trajectory tracking control performance with AMBs under different reference signals based on axial variable reference positional control of the rotor, which is the basis of machining or fluid mechanical surge control. The implementation process of this study is as follows. First, the working principle of trajectory tracking about magnetic bearings is expounded. Then, an integrative electromechanical model of trajectory tracking is comprehensively described and mathematical models of a rotor-electromagnet, sensor, power amplifier, and controller time delay are analyzed. A simulation study based on trajectory tracking of magnetic thrust bearings is then carried out. In the simulation, a PID controller is used to realize trajectory tracking simulation analysis under different reference signals. Finally, the trajectory tracking control performance of different reference signals under static and rotational states is verified experimentally.

The rest of this paper is arranged as follows. Section 2 introduces the AMB trajectory tracking principle. Mechatronics modeling of trajectory tracking is presented in Section 3. Section 4 presents an analysis of the simulation. Section 5 presents the experimental results. Conclusions are drawn in the final section.

II. PRINCIPLE OF MAGNETIC SUSPENSION TRAJECTORY TRACKING

The principle of magnetic suspension trajectory tracking is graphically represented in Fig. 1, where C_0 is the unilateral air gap (C_0 = 0.75 mm), δ represents the offset relative to the middle position, I_0 is the bias current, and I_1 is the control current. The basic working principle is that both the bias current and control current enter the coil, which drives the electromagnet to generate an electromagnetic force. Thus, the value of δ is adjusted to implement trajectory tracking.

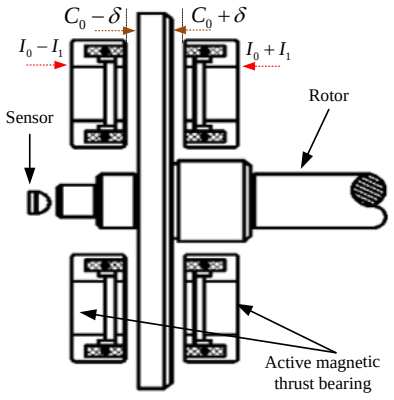

Fig. 1. Principle of magnetic suspension trajectory tracking.

According to Maxwell's principle, the electromagnetic force imposed on a suspended object (rotor) is given by [9]:

$$F_x = F_{x1} - F_{x2} = \frac{\mu_0 AN^2}{4}\left[\left(\frac{I_0+I_1+i_x}{C_0+\delta+x}\right)^2 - \left(\frac{I_0-I_1-i_x}{C_0-\delta-x}\right)^2\right], \quad (1)$$

where F_{x1} and F_{x2} are the electromagnetic forces imposed on the suspended object (rotor) on each side of the magnetic bearing, μ_0 is the permeability of the vacuum, A is the magnetic pole area, N is the number of coils turns, i_x is the current disturbance, and x is the displacement disturbance around the suspension position.

The function is expanded in Taylor's series when $i_x = 0$ and $x = 0$, and neglecting the higher-order term [9]:

$$\tilde{F}_x = \tilde{F}_0 + k_i \cdot i_x + k_x \cdot x, \quad (2)$$

where k_i and k_x indicate the force-current stiffness and force-displacement stiffness, respectively. The parameters in Eq. (2) are given as follows:

$$\tilde{F}_0 = \frac{\mu_0 AN^2}{4}\left[\left(\frac{I_0+I_1}{C_0+\delta}\right)^2 - \left(\frac{I_0-I_1}{C_0-\delta}\right)^2\right], \quad (3)$$

$$k_i = \frac{\mu_0 AN^2}{2}\left[\frac{(I_0+I_1)}{(C_0+\delta)^2} + \frac{(I_0-I_1)}{(C_0-\delta)^2}\right], \quad (4)$$

$$k_x = -\frac{\mu_0 AN^2}{2}\left[\frac{(I_0+I_1)^2}{(C_0+\delta)^3} + \frac{(I_0-I_1)^2}{(C_0-\delta)^3}\right]. \quad (5)$$

When the system is suspended stably, the current disturbance i_x and displacement disturbance x around the suspension position are both zero, and the system is force-balanced, that is:

$$\frac{\mu_0 AN^2}{4}\left[\left(\frac{I_0+I_1}{C_0+\delta}\right)^2 - \left(\frac{I_0-I_1}{C_0-\delta}\right)^2\right] = 0. \quad (6)$$

Finally, it can be deduced that $I_1 = \frac{\delta}{C_0} I_0$.

Both the force-current stiffness k_i and force-displacement stiffness k_x can be considered as nonlinear functions of the offset value relative to the middle position δ.

According to the parameters in Table 1, the relationships between the force-current stiffness k_i, the force-displacement stiffness k_x, and the offset relative to the middle position δ can be obtained, as shown in Fig. 2.

Variation in the electromagnetic force of the AMBs requires adjustment of the active controller. Thus, stable suspension and accurate trajectory tracking of the rotor

can be obtained. The control principle is depicted in Fig. 3. The error between the reference signal and feedback signal (that is, the trajectory tracking signal) is actively adjusted by the controller, with the target error being zero. If the error is not zero, the controller will keep actively adjusting the system. This adjustment process comprises the trajectory tracking of the AMBs.

Table 1: Major parameters of the magnetic thrust bearing

Parameter Name	Symbol	Value	Unit
Vacuum permeability	μ_0	$4\pi\times10^{-7}$	N/A^2
Magnetic pole area	A	7.69×10^{-4}	m^2
Coil turns	N	240	/
Single stage clearance of middle point	C_0	0.75×10^{-3}	m
Bias current	I_0	2.0	A

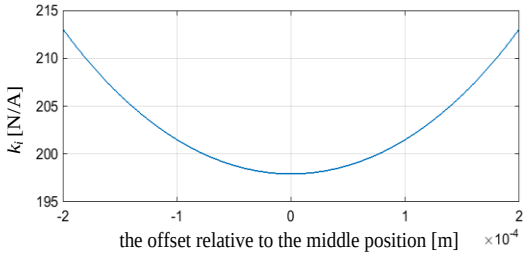

(a) Variation in force-current stiffness with suspension position

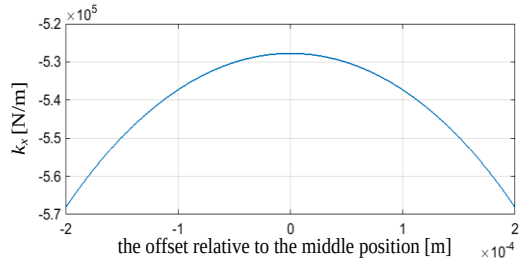

(b) Variation in force-displacement stiffness with suspension position

Fig. 2. Relationships of force-current stiffness k_i and force-displacement stiffness k_x.

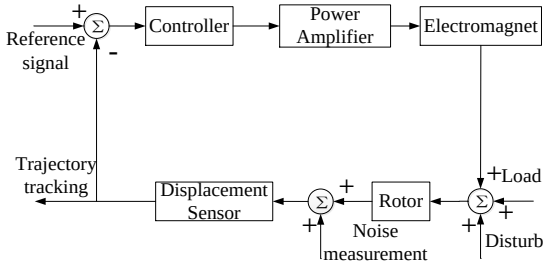

Fig. 3. Principle of trajectory tracking in AMBs.

Because variation in the suspension position can lead to changes in the force-current stiffness k_i and force-displacement stiffness k_x, it is necessary to determine whether the controller can ensure system stability and good tracking under changing values of k_i and k_x.

III. MODELING OF AMB TRAJECTORY TRACKING

The AMB trajectory tracking control model is depicted in Fig. 4. Displacement of the rotor relative to the reference position is detected by the sensor. The control signal is calculated by the controller according to the error signal. The control signal is sent to the power amplifier to be transformed into the control current, which will drive the electromagnet to generate the control force so that the rotor is suspended in a given position. In Fig. 4, C is the controller, K_a is the transfer function of the power amplifier, G_{AMB} is the transfer function of the electromagnet and rotor, and K_s is the gain of the sensor.

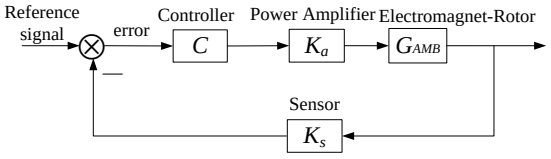

Fig. 4. Control model of trajectory tracking.

A. Electromagnet-rotor model

Around the stable working point of the magnetic bearing system, the transfer function of the electromagnet and rotor can be determined by small-scale linearization of force, displacement and current [9]:

$$G_{AMB} = \frac{k_i}{ms^2 + k_x}, \tag{7}$$

where m represents the rotor mass (m = 14.56 kg).

B. Displacement sensor model

The bandwidth of the eddy current displacement sensor is 5 kHz, which is much larger than the frequency of the axial tracking signal. Therefore, the displacement sensor can be considered as an ideal proportional system. The detection range of the axial displacement sensor is 0 to 0.9 mm and its output ranges from 0 to 5 V. The gain of the sensor is given by:

$$K_s = 50000/9 \ \text{(V/m)}. \tag{8}$$

C. Power amplifier model

The adopted power amplifier is a kind of voltage-current three-level PWM switching power amplifier. After obtaining the amplitude-frequency characteristics of the power amplifier by a frequency sweep test, the

transfer function can be identified by a third-order model:

$$K_a = \frac{0.04204s^3 + 3979s^2 + 8.737\times10^6 s + 1.505\times10^9}{s^3 + 9251s^2 + 6.451\times10^6 s + 1.098\times10^9}. \quad (9)$$

Figure 5 illustrates a comparison of the tested frequency response and the theoretical model of the power amplifier. The red solid line is the Bode diagram of the theoretical model, namely Eq. (9), and the blue dashed line is the Bode diagram of the experimental test. From this figure, it can be seen that the theoretical model accurately describes the characteristics of the power amplifier.

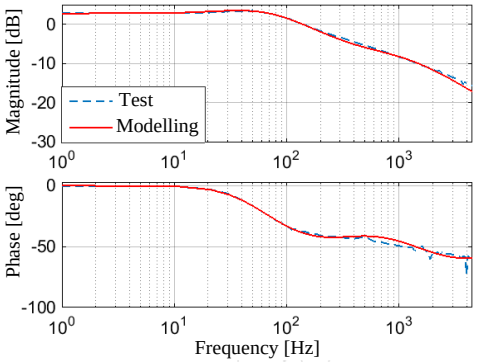

Fig. 5. Comparison between the tested frequency response and theoretical model of the power amplifier.

D. Modeling of the electrical part of the system

The digital control system was developed based on DSP. Its hardware included an anti-aliasing filter circuit added to the pre-processing circuit before the displacement input, and a smoothing filter was added to the post-processing circuit after the control signal. As for the DSP chip itself, A/D and D/A conversion were also added into the control system.

The transfer functions of the smooth filter link and partial voltage link were obtained by theoretical derivation, as follows:

$$G_{pp}(s) = \frac{0.6}{9.132\times10^{-10}s^2 + 4.22\times10^{-5}s + 1}. \quad (10)$$

The mathematical models of the DSP chip and D/A conversion module can be simplified to time delay transfer functions, and the mathematical model of the DSP chip and D/A transfer module can be obtained as:

$$G_D(s) = k_d e^{-sk_t T_s}. \quad (11)$$

In Eq. (11), k_t is the coefficient of lag time and k_d is the gain term. A more accurate mathematical model can be obtained by modifying k_t and k_d. In this paper, the approximate mathematical model can be obtained by adopting a second-order Pade approximation [17]. Taking k_t as 1.1, k_d as 3.35, and sampling time T_s as 0.0001, an approximate mathematical model of the time delay can be obtained as follows:

$$G_D(s) \approx k_d \frac{(0.3175T_s s - 1)^2}{(0.3175T_s s + 1)^2} = \frac{3.35(0.3175\times10^{-4}s - 1)^2}{(0.3175\times10^{-4}s + 1)^2}. \quad (12)$$

E. Reducing the order of the overall object model

After getting the model of each link in the trajectory tracking closed-loop, all links except the controller are incorporated into the controlled object, then the model of the controlled object is as follows.

$$G_s(s) = G_{AMB}(s)\bullet K_s(s)\bullet K_a(s)\bullet G_{pp}(s)\bullet G_D(s). \quad (13)$$

The order of the controlled object model is 10, and such high order number will make it difficult to adjust the controller parameters in the simulation. Thus, the control algorithm is hard to implement. Since the operating frequency range of the magnetic thrust bearing-rotor system mainly covers lower frequencies, the order of the controlled object model can be reduced if the accuracy of the system at low frequencies can be guaranteed. We used the hankelmr function to reduce the order of the model to 3. The model after reduction is given by:

$$G_s(s) = \frac{-11.47s^2 + 2.389\times10^4 s + 1.436\times10^8}{s^3 + 557.3s^2 - 1.101\times10^4 s - 2.501\times10^7}. \quad (14)$$

IV. SIMULATION OF TRAJECTORY TRACKING

The electromagnetic force of the magnetic suspension fluid mechanical rotor and the magnetic suspension machining tool will change nonlinearly with changes of the suspension position. In order to study the trajectory tracking performance of the magnetic bearing system, a PID controller was designed.

The structure of the PID controller is presented in Eq. (15), and its control parameters, obtained by trial-and-error, are illustrated in Table 2:

$$C(s) = K_p + \frac{K_i}{s} + K_d \frac{s}{\frac{1}{2\pi f}s + 1}. \quad (15)$$

Table 2: Control parameters of the PID controller in simulation

Control Parameter	Symbol	Value
Proportional coefficient	K_p	9
Integral coefficient	K_i	90
Differential coefficient	K_d	0.03
Cut-off frequency	f	1500

A reference signal is introduced into the sinusoidal signal with a frequency is 0.5 Hz and amplitudes of 0.2 V, 0.4 V, and 0.6 V, respectively. The obtained simulation of rotor position tracking is shown in Fig. 6. It can be seen from Fig. 6 that sinusoidal signals of different amplitudes have better tracking performance with a 0.5 Hz frequency. Moreover, the tracking error of the

sinusoidal signals with different amplitudes is almost the same, with a maximum value of about 0.58%.

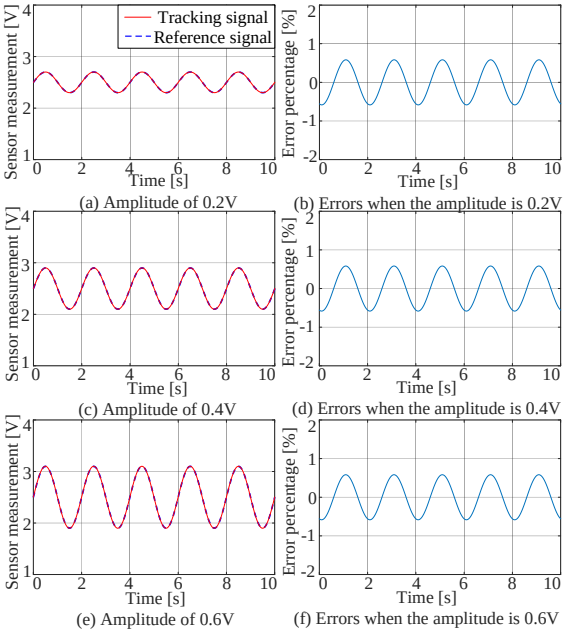

Fig. 6. Trajectory tracking of sinusoidal signals.

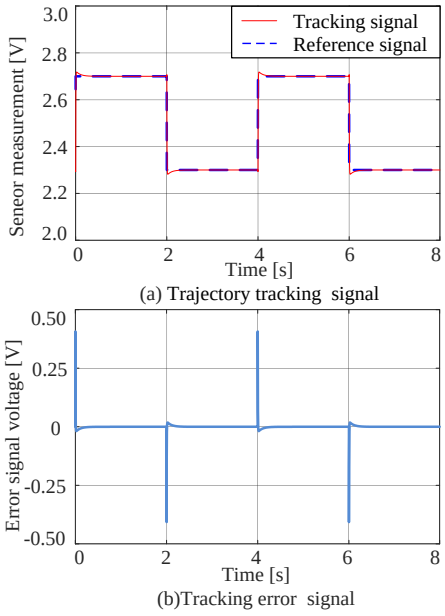

Fig. 7. Trajectory tracking of square wave signal.

The reference signal is superposed with a square wave signal with a frequency of 0.25 Hz and amplitude of 0.4 V so that a trajectory tracking simulation of the rotor can be obtained, as presented in Fig. 7. It can be seen from Fig. 7 that the square wave signal also has good tracking performance. The maximum tracking error occurs at the moment of sudden change in the signal. However, the error of the maximum amplitude relative to the equilibrium position is small, which is about 0.018V, and the adjustment time is about 0.32 seconds.

The reference signal is set to a continuous step form to achieve trajectory tracking simulation of the rotor, as illustrated in Fig. 8. From Fig. 8, we can see that the tracking effect is better with the continuous step signal. The maximum tracking error also occurs at the moment of sudden change in the reference signal. The error of the maximum amplitude relative to the equilibrium position is relatively small, which is 0.01 V. The adjustment time is only 0.19 seconds.

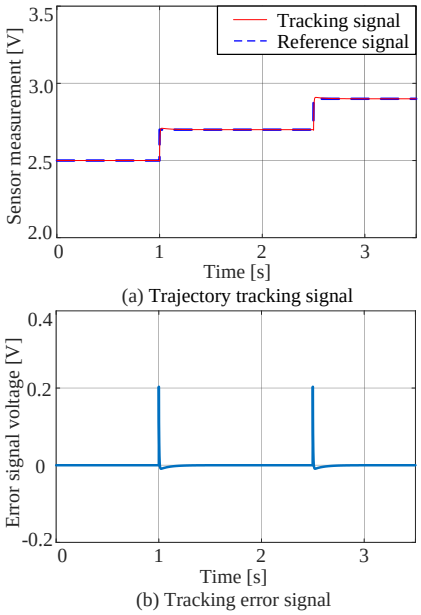

Fig. 8. Trajectory tracking of a continuous step signal.

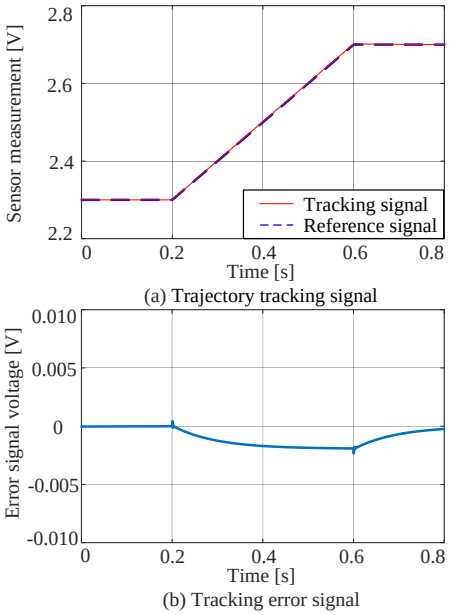

Fig. 9. Trajectory tracking of a ramp signal.

Figure 9 displays the tracking performance of a ramp signal. It can be concluded that since the variation amplitude of the signal transition is smaller than that of the square wave and step signals, the tracking error is relatively small, with a maximum tracking error of about 0.0024 V.

V. EXPERIMENTAL STUDY OF TRAJECTORY TRACKING PERFORMANCE

In this section, the tracking effect of different reference signals is verified by the axial trajectory tracking experiments under the static suspension and rotating states.

A. Trajectory tracking performance under a static suspension state

Figure 10 shows the test rig, whose main components were an AMB-rotor test bench, sensors and conditioning circuit, power amplifiers, digital controller, signal generator, PC, and so on. Table 3 lists the PID control parameters used in the experiment.

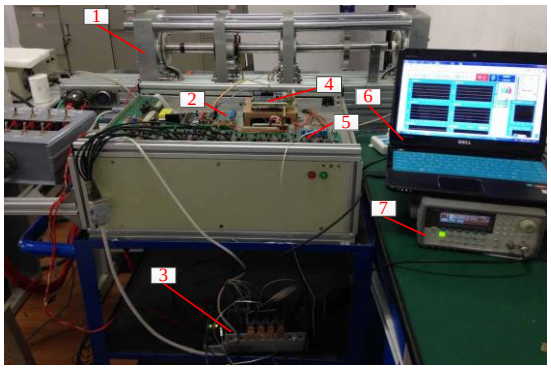

1.AMB-Rotor; 2.Sensors and conditioning circuit; 3.Data acquisition card; 4.Digital controller; 5.Power amplifier; 6. PC; 7.Signal Generator.

Fig. 10. Experimental equipment.

Table 3: PID controller parameters used in the experiment

Control Parameter	Symbol	Value
Proportional coefficient	K_p	7
Integral coefficient	K_i	70
Differential coefficient	K_d	0.0192
Cut-off frequency	f	1500

The signal generator generated sinusoidal signals with a frequency of 0.5 Hz and amplitudes of 0.2 V, 0.4 V, and 0.6 V. The signals were input to the digital controller of the magnetic bearing system as an axial position reference signal to obtain the axial position response of the rotor, as shown in Fig. 11.

From Fig. 11, it can be concluded that the positional tracking errors of the sinusoidal signals under PID control were small and meet the basic real-time tracking requirements. Due to the existence of high-frequency interference, the tracking errors were slightly larger than those of the simulation. The error was about 20% at an amplitude of 0.2 V and was within 15% at amplitudes of 0.4 V and 0.6 V. The larger error at the lower amplitude was also due to the existence of high-frequency interference, which increases the relative error at low amplitude.

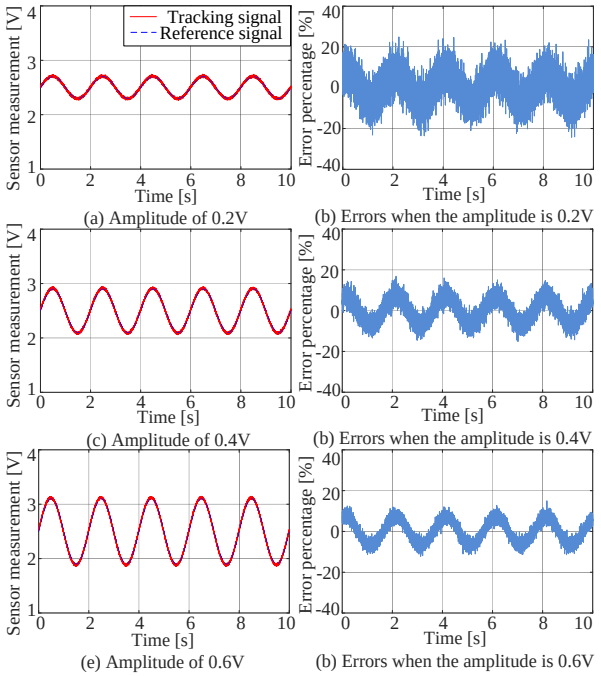

Fig.11. Trajectory tracking of sinusoidal signals (static suspension).

Figure 12 exhibits the tracking performance with a square wave reference signal. The reference signal was superimposed with a square wave signal with a frequency of 0.25 Hz and amplitude of 0.4 V. From Fig. 12, it is evident that the square wave signal also provided a good tracking effect in the experiment. The maximum tracking error occurred at the moment of abrupt change, but the error of the maximum amplitude relative to the equilibrium position was small, about 0.18 V, and the adjustment time was about 0.17 seconds.

The reference signal was set to a continuous step form, as illustrated in Fig. 13, and a rotor position tracking effect diagram was obtained. It can be observed from Fig. 13 that the continuous step signal had a good tracking effect. The maximum tracking error was at the moment of sudden change in the step signal. The errors of the maximum amplitude relative to the equilibrium position and adjustment time were small, about 0.12 V and 0.17 seconds, respectively.

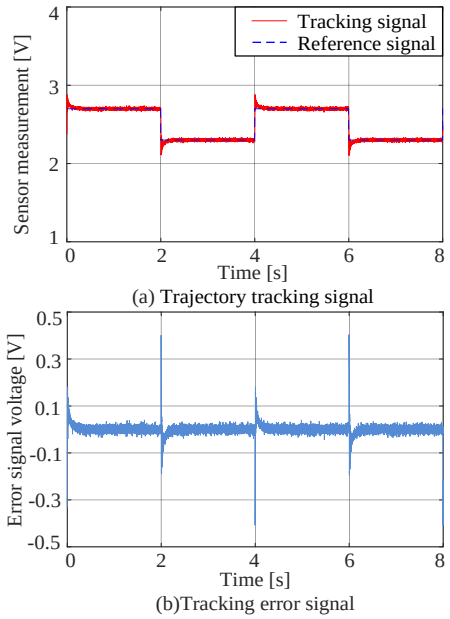

Fig. 12. Trajectory tracking of a square wave signal (static suspension).

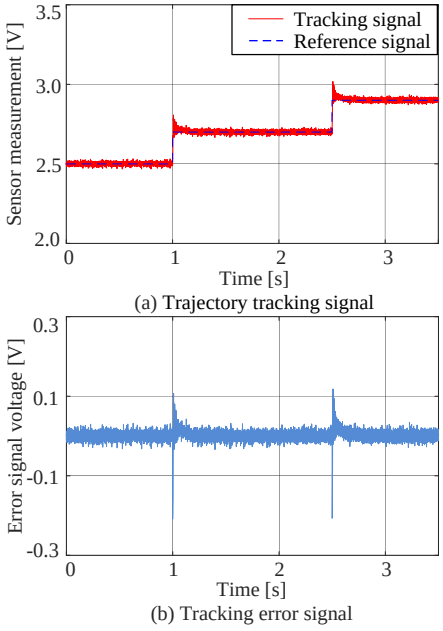

Fig. 13. Trajectory tracking by a continuous step signal (static suspension).

Fig. 14 shows a tracking effect diagram for a ramp reference signal. Similar to the simulation results, the error was smaller than with other mutation signals. The tracking effect meets the basic real-time tracking requirements.

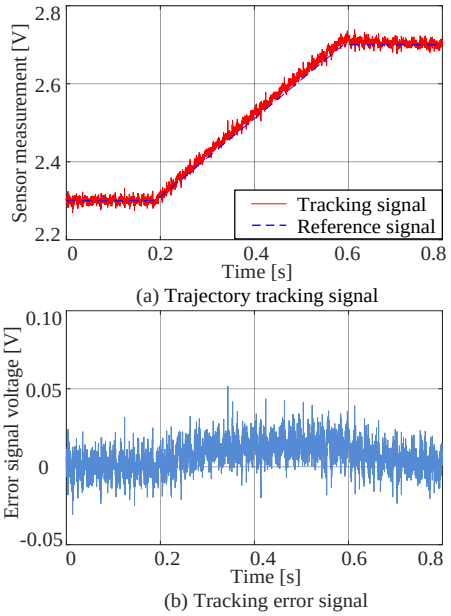

Fig. 14. Trajectory tracking by a ramp signal (static suspension).

The experimental results above indicate that the system had good axial position tracking performance under static suspension. However, the tracking performance in a rotating state still needs verification.

B. Trajectory tracking performance in a rotating state

The trajectory tracking accuracy of the magnetic bearing spindle system in the rotating state is directly related to the machining accuracy of the workpiece. And the magnetic suspended fluid mechanical surge control is also operated under the rotating state. So, it is particularly important to study the tracking accuracy in the rotating state. The tracking performance of sinusoidal signals at different rotational speeds is shown in Fig. 15. It can be indicated from Fig. 15 that the performance of the positional tracking of the magnetic bearing system was less affected by the rotational speed, with maximum errors of about 30% at the three speeds tested. The main reason for the larger error is that the amplitude of the sinusoidal reference signal was 0.2 V (too small for high-frequency noise) at the three speeds, and the final error was relatively large due to the existence of high-frequency noise.

To study the trajectory tracking performance of the magnetic bearing system while rotating, a speed of 3000 rpm was selected for the experiment. The tracking results with a sinusoidal signal with amplitudes of 0.4 V and 0.6 V are shown in Fig. 16. Compared with tracking during static suspension (Fig. 11), tracking while rotating was also good, with an error was less than 15% (Fig. 16).

Taking the sinusoidal signal with an amplitude of 0.6 V as an example, the tracking error was within 16.2 μm. It is also evident that the larger the amplitude of the sinusoidal signal, the smaller the tracking error. The reason is that the existence of high-frequency noise affects the tracking accuracy of low amplitude signals.

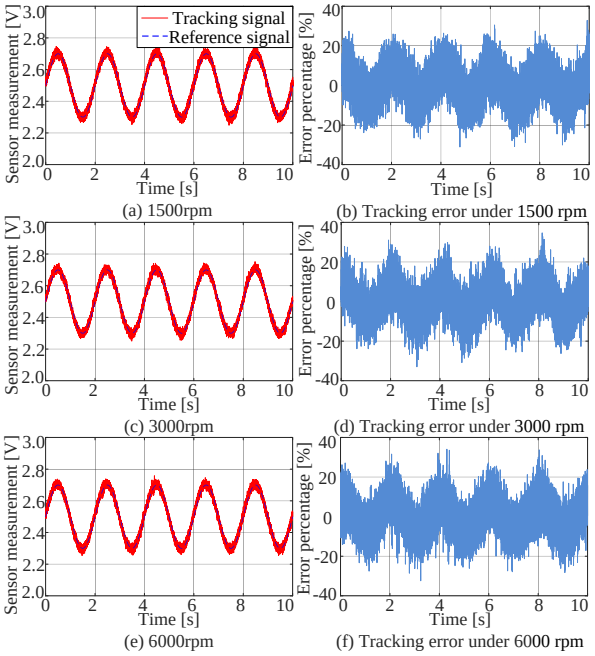

Fig. 15. Tracking by sinusoidal signals in a rotating state.

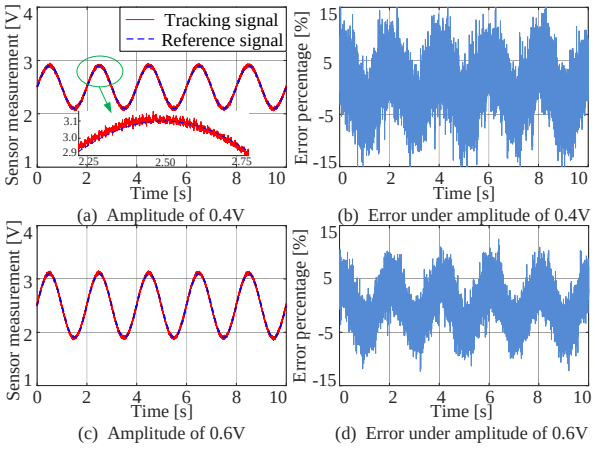

Fig. 16. Tracking by sinusoidal signals (3000 rpm).

Figure 17 displays the tracking performance with a square wave signal at a bearing speed of 3000 rpm. It shows that the tracking effect was better in the rotating state and the maximum error occurred at the position of signal mutation.

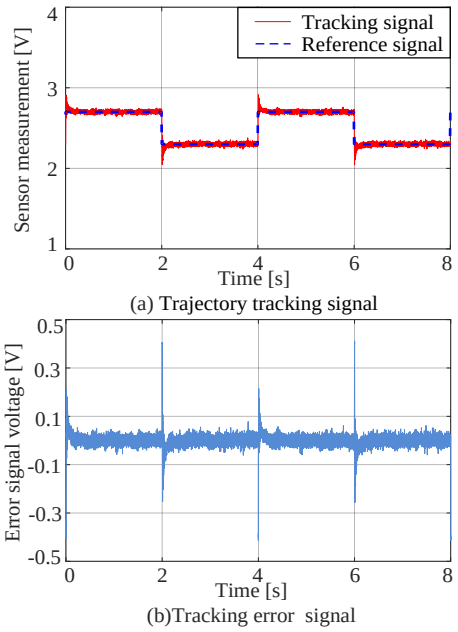

Fig. 17. Tracking by a square wave signal (3000 rpm).

The tracking performance with a continuous step signal at 3000 rpm is illustrated in Fig. 18. The tracking error was within ± 0.1 V, which is about 18 μm.

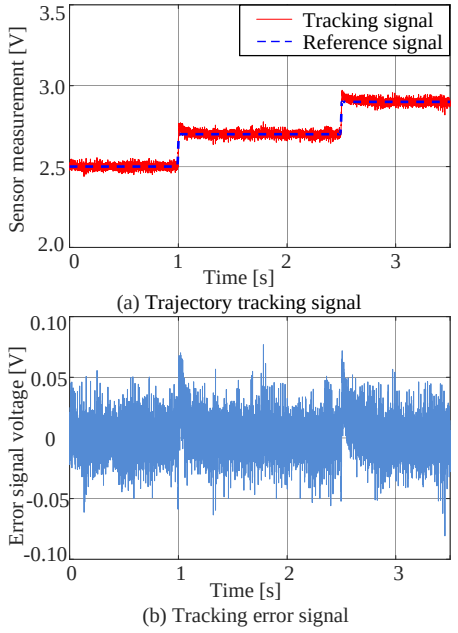

Fig. 18. Tracking by a continuous step signal (3000 rpm).

Figure 19 illustrates the tracking performance with a ramp signal at 3000 rpm. The tracking error was within ± 0.05 V, which is about 9 μm.

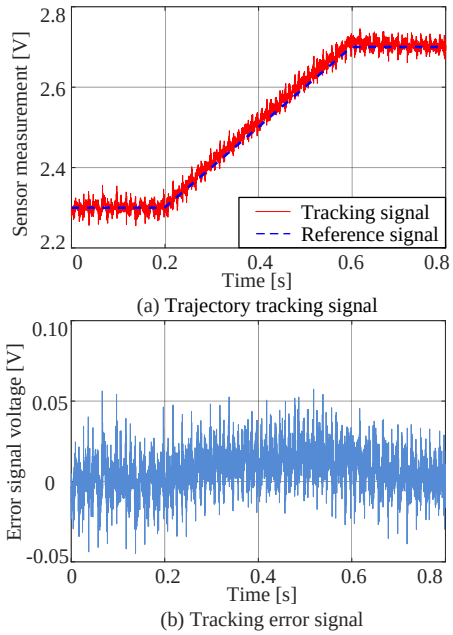

Fig. 19. Tracking by a ramp signal (3000rpm).

The results of the rotational tracking experiments demonstrate that axial position tracking was better, and all tracking errors were small with different machining contours.

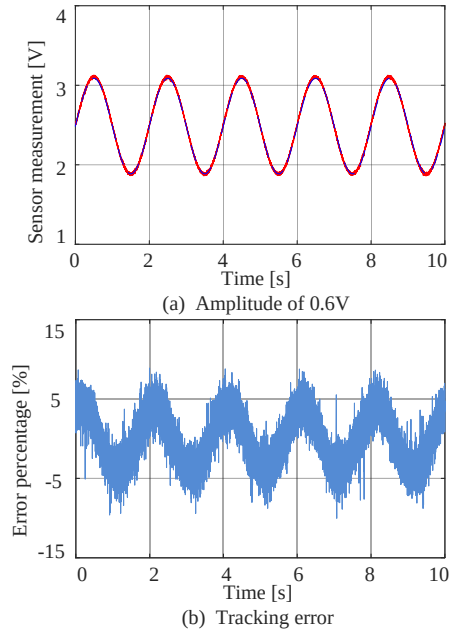

Fig. 20. Tracking by sinusoidal signals with a low-pass filter (3000 rpm).

In order to reduce the influence of sensor measurement noise, a displacement signal was input to the controller after it passed through the second-order low-pass filter with a cut-off frequency of 3 kHz, and then the corresponding control was performed. The transfer function of the low-pass filter was as follows:

$$G_s(s)=\frac{1}{1.1501\times10^{-9}s^2+6.7827\times10^{-5}s+1}. \quad (16)$$

Taking the 0.6 V sinusoidal signal in Fig. 16 as an example, the tracking effect after introducing the low-pass filter is shown in Fig. 20. The comparison shows that the low-pass filter effectively reduced the high-frequency component of the displacement signal. At the same time, the error was reduced by about 2.3% compared with the original.

The lower the cut-off frequency, the lesser the influence of displacement signal noise on the controller, but an over-lowed cut-off frequency reduces the stability of the system. Therefore, an effective cut-off frequency should be obtained via repeated experiments.

VI. CONCLUSION

In this paper, we abstracted the machining curve into several different reference signals. Then, the trajectory tracking performance of the magnetic thrust bearing under these reference signals was studied. Simulations and experiments indicate that the PID controller can meet the performance requirements of axial position control, and the trajectory tracking errors are within the allowable range. All the different machining profiles tested in this paper can meet the requirements of positional control. The results obtained in this paper provide bases for the positional control of magnetic levitation motorized spindle tools and magnetic suspension fluid mechanical surge control. The conclusions are summarized as follows.

1) Both static and rotating states provide high trajectory tracking accuracy, but the accuracy is slightly lower in the rotating state.
2) Rotational speed has little effect on the accuracy of axial trajectory tracking.
3) High-frequency noise causes relatively large tracking errors with reference signals with small amplitudes.
4) Tracking accuracy based on sinusoidal signals is higher than that using other signals such as square waves.
5) Overall, under the experimental conditions, the tracking errors were all within 18 μm.
6) After the low-pass filter was introduced, the high-frequency component of the displacement signal could be significantly reduced.

In future work, we will study trajectory tracking with different interference signals and try to improve tracking accuracy by applying advanced algorithms. Reducing the influence of high-frequency noise on tracking accuracy is also worthy of further research.

ACKNOWLEDGMENT

This work has been supported by National Natural Science Foundation of China (51675261), Jiangsu Province Key R&D programs (BE2016180), Postgraduate Research & Practice Innovation Program of Jiangsu Province (KYCX17_0244).

REFERENCES

[1] M. Tang, J. Zhou, C. Jin, and Y. Xu, "Vibration isolation of magnetic suspended platform with double closed-loop PID control," *Applied Computational Electromagnetics Society Journal*, vol. 32, no. 8, pp. 712-719, 2017.

[2] K. Sato and G. J. Maeda, "A practical control method for precision motion-Improvement of NCTF control method for continuous motion control," *Precision Engineering*, vol. 33, no. 2, pp. 175-186, 2009.

[3] H. Shi, D. Zhang, J. Yang, C. Ma, and G. Gong, "Experiment-based thermal error modeling method for dual ball screw feed system of precision machine tool," *International Journal of Advanced Manufacturing Technology*, vol. 82, pp. 1693-1705, 2016.

[4] A. Woronko, J. Huang, and Y. Altintas, "Piezoelectric tool actuator for precision machining on conventional CNC turning centers," *Precision Engineering*, vol. 27, no. 4, pp. 335-345, 2003.

[5] Y. Tian, B. Shirinzadeh, and D. Zhang, "A flexure-based mechanism and control methodology for ultra-precision turning operation," *Precision Engineering*, vol. 33, no. 2, pp. 160-166, 2009.

[6] S. Eckhardt and J. Rudolph, "High precision synchronous tool path tracking with an AMB machine tool spindle," *The 9th International Symposium on Magnetic Bearings*, Lexington, KY, USA, 2004.

[7] H. Wang and D. Hu, "Machining principle for noncircular piston pin-hole based on magnetic levitated spindle," *Chinese Internal Combustion Engine Engineering*, vol. 27, no. 3, pp. 54-57, 2006.

[8] A. Smirnov, A. H. Pesch, O. Pyrhönen, and J. T. Sawicki, "High-precision cutting tool tracking with a magnetic bearing spindle," *Journal of Dynamic Systems Measurement & Control*, vol. 137, no. 5, pp. 1-8, 2015.

[9] G. Schweitzer and E. H. Maslen, *Magnetic Bearings*. Springer, Berlin, Germany, 2009.

[10] D. Sanadgol, "Active control of surge in centrifugal compressors using magnetic thrust bearing actuation," *Virginia: University of Virginia*, 2006.

[11] S. Y. Yoon, "Surge control of active magnetic bearing suspended centrifugal compressors," *Virginia: University of Virginia*, 2011.

[12] T. P. Minihan, S. Lei, G. Sun, A. Palazzolo, A. F. Kascak, and T. Calvert, "Large motion tracking control for thrust magnetic bearings with fuzzy logic, sliding mode, and direct linearization," *Journal of Sound and Vibration*, vol. 263, no. 3, pp. 549-567, 2003.

[13] A. H. Pesch, A. Smirnov, O. Pyrhönen, and J. T. Sawicki, "Magnetic bearing spindle tool tracking through μ-synthesis robust control," *IEEE/ASME Transactions on Mechatronics*, vol. 20, no. 3, pp. 1448-1457, 2015.

[14] S. Zheng, J. Yang, X. Song, and C. Ma, "Tracking compensation control for nutation mode of high-speed rotors with strong gyroscopic effects," *IEEE Transactions on Industrial Electronics*, vol. 65, no. 5, pp. 4156-4165, 2018.

[15] T. R. Grochmal and A. F. Lynch. "Precision tracking of a rotating shaft with magnetic bearings by nonlinear decoupled disturbance observers," *IEEE Transactions on Control Systems Technology*, vol. 15, no. 6, pp. 1112-1121, 2007.

[16] S. Basovich, S. Arogeti, and Z. Brand, "Adaptive output zero-bias tracking control of 1DOF AMB suspension system," *International Conference on Control Automation Robotics & Vision IEEE*, pp. 151-156, 2014.

[17] S. Skogestad and I. Postlethwaite, *Multivariable Feedback Control: Analysis and Design*. Wiley, New York, USA, 2005.